# Machine learning techniques for the prediction of polymerization kinetics and polymer properties

Niyi B Ishola, Timothy F L Mckenna

# Machine Learning Techniques for the Prediction of Polymerization Kinetics and Polymer Properties.

*Niyi B. Ishola*[*,§], Timothy F.L. McKenna*

CP2M-UMR 5128, Université de Lyon, Bâtiment CPE-Lyon, 43 Blvd du 11 Novembre 1918, F-69616 Villeurbanne, France

*isholaniyi10@gmail.com

[§]Present address: Innotech Process Technology, Borealis Polymers PO PDO, Borealis Polymers Oy, P.O. Box 330, Porvoo, Finland

## Abstract

In the current study, the ability of two data-driven machine learning tools, the extreme learning machine (ELM) and the adaptive neuro-fuzzy inference system (ANFIS), to predict the polymerization rate and melt flow index of linear low-density polyethylene produced in a gas phase process was investigated. The level of interaction between the input variables (ethylene, 1-butene, isopentane pressures, and reaction temperature) on the outputs (melt flow index and activity) was also examined. It was found that both outputs are impacted by the presence of isopentane as an induced condensing agent. Various statistical indicators, including the coefficient of correlation ($R^2$) and root mean square error (RMSE), were used to quantitatively evaluate both developed models. The ANFIS model outperformed the developed ELM model in terms of predicting the MFI and the catalyst activity. A sensitivity analysis of the ANFIS and ELM models showed that all the input variables under investigation had a sizable impact on the responses and none of them could have been discarded. The present study showed that machine learning tools could be employed to adequately develop empirical models to predict polymerization kinetics as well as the final polymer properties.

keyword: modeling, statistics, machine learning, surface plots, LLDPE, induced condensing agents.

## 1 INTRODUCTION

The variety of polyolefin grades currently in the market is the consequence of advancement in both the development of good catalytic systems such as Ziegler-Natta (ZN) and metallocenes as well as the utilization of new reactor configurations and operating conditions [1]. In terms of annual tonnage, polyethylene is the most widely produced synthetic polymer worldwide, with a global market value of approximately 110 billion dollars at the time this article was written. Furthermore, it is expected that this figure will increase to over 146 billion dollars by 2030 [2]. Our ability to fine-tune the macromolecular architecture of these extremely basic polymers, which only include carbon and hydrogen, is what has led to this accomplishment. Precise control of properties comes from developments in both

polymerization catalysts (except for low density polyethylene, LDPE which is made by a free radical process), and in the design and operation of polymerization reactors [3].

Commercially, the most popular method for producing linear low density polyethylene (LLDPE) is gas phase ethylene polymerization using supported catalysts in fluidized bed reactors (FBR). The highly porous particles used in this method typically have a diameter of a few tens of microns, and the active catalytic sites are accessible on the surface of the pores [3]. Following the introduction of the catalyst into the reactor, ethylene, comonomer and other compounds diffuse through the pores to the active sites where the polymer is formed. The first layer of polymer immediately covers the active sites, and once this layer is formed, the gas phase components must first dissolve in the polymer, through which they are transported to the active sites where polymerization takes place. After a period of time, on the order of seconds to tens of seconds, enough polymer accumulates in the particles that the resulting hydraulic pressure causes the initial support material to fragment, but the accumulated polymer (hopefully) maintains the physical integrity of the original particle [3]. This fragmentation step is quite important as it contributes to determining the particle morphology, and thus the relevant length scales for the diffusion of gas phase components through the amorphous phase of the resulting semi-crystalline polymer [4].

In order to be commercially successful, it is necessary to operate at very high catalyst activities. Since this type of polymerization is highly exothermic, one of the main challenges here is the evacuation of the enthalpy of polymerization. By introducing inert alkanes of carbon atoms ranging from 3 to 6 to the gas phase feed stream at the bottom of the reactor, the heat removal capacity of FBR can be significantly increased. These substances are typically referred to as induced condensing agents (ICAs), and the reactor is said to be operating in condensed mode if the recycle stream containing these inert alkanes is cooled to a temperature below its dew point [5; 6]. When multiple components are present in the gas phase, the resulting gas-polymer equilibrium can be quite complex, with the concentration of different species at the active sites being a function not just of the partial pressure of said species, but also of the concentration of other species in the amorphous phase of the polymer. The enhancement of ethylene concentration in the amorphous phase of the polymer (and its diffusivity in this phase) by heavier species (e.g. comonomer or ICA) is referred to as the cosolubility effect, and the reduction of the solubility and diffusivity of these heavier species by ethylene (and other light components) is referred to as the antisolvent effect [6; 7]. The cosolubility impact not only accelerates polymerization but also affects reactor behavior [8],

rate of crystallization [9], the morphology of particles, molecular weight distribution, and crystallinity [7; 10]. It has recently been demonstrated that the presence of these ICAs could also impact how the reactivity ratios are estimated for copolymerization systems [11].

Due to the complexity of the underlying physical processes, it is very difficult to develop models that can describe their influence on the observed kinetics [12]. For instance fragmentation can influence mass transfer resistance, but ICA that enhance diffusivities [13; 14] can also plasticize the polymer as the particles fragment and grow, and thus influence the morphology as well and this is without worrying about whether or not we can predict the heat removal rates from the particle during the polymerization [15]. For more on this, the interested readers are referred to references [4; 16]. This tells us that it can be challenging to pinpoint all the potentially significant interactive effects that operating variables may have, particularly on the pertinent responses involve during polymerization reaction. In the absence of reliable mechanistic models of the process it is advantageous to explore and develop alternative strategies for comprehending these interactions.

A statistical tool such as response surface methodology (RSM) is often employed to illustrate the relationship between the various operating parameters as well as the synergistic effect of different operating variables on the outputs due to its simplicity. For examining multivariate issues like polymerization and identifying the end products, as well as for figuring out relationships between the two, RSM is a very useful technique [17; 18]. RSM has been successfully employed in polymerization processes [19-22]. However, recent studies comparing the predictive capability of RSM and artificial neural networks (ANN) showed that ANN has better predictive and generalization capability than RSM [23]. ANN is a type of neural intelligence technique that is based on data-driven machining learning techniques capable of predicting the various responses for a particular chemical process. It has been successfully applied to investigate and improve ethylene polymerizations catalyzed by single site catalyst [24; 25], to predict the performance of ethylene polymerization over novel metallocene/post-metallocene multisite catalyst [26], and also employed to predict polymerization kinetics and final polymer properties of polyethylene using ZN catalyst [23]. It has also been reported to have successfully application in reactive extrusion technology to handle nonlinearity in the process [27]. However, conventional ANNs have several disadvantages due to their learning process limitations, including the existence of multiple local minima, slow learning rate, and large training datasets [28]. As a result, the use of other neural intelligence techniques such as

neuro-fuzzy inference systems and extreme learning machines has been gaining attention recently [28; 29].

ELM uses a single hidden layer feedforward neural network (SLFN) as its training algorithm, which produces a performance that is promising and allows for faster convergence than traditional methods. ELM is a technique that was first presented for generalized SLFNs and has been applied to modeling and optimization in some engineering disciplines. The hidden layer parameters are modified at random while the response weights are determined by the generalized inverse function developed by Moore-Penrose. The ELM has a single layer of hidden nodes with arbitrarily assigned weights between inputs and hidden nodes. As a result, the parameters of the models can be calculated without the need for a learning process, and they remain constant throughout the training and prediction stages [30].

ANFIS is a hybrid artificial intelligence that combines fuzzy logic and neural networks. It is also referred to as the neuro-fuzzy. It is a combined system that benefits from the learning abilities of both fuzzy systems and neural networks [31]. As a result, the neural network has been made explicit, enabling fuzzy systems to acquire new skills. Additionally, a neuro-fuzzy system has the capacity to generate a solid set of fuzzy IF-THEN rules from a representative sample of the instances under study [32]. ANFIS can deliver effective outcomes when the right number of rules are utilized, together with effective parameter training. ANFIS's adaptability, speed, and robustness have encouraged its use in a variety of academic fields, including engineering, medicine, and economics.

While ELM and ANFIS have been widely employed in various chemical processes, there has been no report on the use of these data-driven machine learning techniques in gas phase ethylene polymerization to test their predictive capability in term of polymer kinetics and final polymer properties. Hence, in this present study, the predictive capability of ELM and ANFIS are presented in accurately prognosticating the activity and melt flow index (MFI) of polyethylene produced from gas phase ethylene polymerization in the presence of isopentane as ICA. The combined effect of the pertinent operating variables (ethylene, 1-butene, isopentane pressures, and reaction temperature) on the activity and MFI was also investigated. Different statistics were used to examine the effectiveness of the two machine learning techniques.

## 2.0 EXPERIMENTAL SECTION

### 2.1 Materials and methods

Argon, hydrogen, and ethylene, all of which had 99.5% purity were obtained from Air Liquide (Paris, France). Before usage, ethylene was purified in three separate columns: the first contained reduced BASF R3-16 catalyst (CuO on alumina), the second contained molecular sieves (13X, 3A, Sigma-Aldrich), and the third contained Selexsorb COS (Alcoa). Air Liquide supplied 1-butene with a minimum purity of 99%. Sigma-Aldrich ICN (Germany) supplied iso-pentane with a minimum purity of 99%, and it was further purified by distillation over $CaH_2$. Triethylaluminium which served as cocatalyst was obtained from Witco (Germany). A commercial $TiCl_4$ supported on $MgCl_2$ Zeigler-Natta catalyst was used for all polymerization operations. The catalyst particles were dispersed in a seedbed of 99% minimum purity NaCl, which was purchased from Carl Roth (Germany). To completely remove any traces of water, the salt was dried under vacuum for 5 h at 400 °C before usage.

### 2.2 Procedure for Polymerization

Following a method previously described [9], gas phase polymerization was carried out using a seedbed of 40 g of dried NaCl in a 2.5 L spherical stirred-bed gas phase reactor. Since the catalyst formulation was not examined in this study, all runs were conducted using 7 mg of Ziegler-Natta catalyst (combined with 10 g of NaCl in the glove box and placed into the cartridge) and 0.6 mL of a 1 M TEA solution in heptane. For a specific set of conditions, each polymerization lasted for 1 h. The reactor was cooled and depressurized once the reaction was finished. The product was removed, thoroughly washed with water, and vacuum-dried at a temperature of 70 °C. Table 1 lists all of the polymerization runs that were taken into consideration along with the experimental measurements. Considered polymerization temperatures range from 70 to 90 °C. The range of pressures taken into account for ethylene (C2) was 7, 8, and 9 bars, and for 1-butene (1-C4) and iso-pentane (iC5) it was 0, 1, and 2 bars. The pressure of hydrogen was maintained at 1 bar. The pressure drop in the feed ballast was used to quantify the rates of polymerization, and the gravimetric yield measurement was used to estimate the value of the activity for a given set of conditions.

### 2.3 Polymer characterization with extrusion plastometer

The MFI of the polymer powders was assessed using the ASTM D1238 test with an extrusion MFI tester (Zwick Roell, Ulm, Germany). About 5 g of polymer sample was melted at 190 °C with a mass of 21.6 kg, and then extruded. To obtain the MFI value, the extrudate was further weighed (on a precision scale of 0.001 g) and standardized by melt flow time, in this case, 10 min.

### 2.4 ELM and ANFIS predictive modeling of gas phase ethylene polymerization

The predictive modeling capabilities of ELM and ANFIS were evaluated in the gas phase ethylene polymerization using a commercial ZN catalyst. Four input variables, (monomer, comonomer, ICA pressure, and reaction temperature) were employed to conduct the polymerization reaction. Different statistics were used to assess the performance of the two approaches. In addition, the relative importance of the analyzed input parameters on the outputs (activity and MFI) is presented.

#### 2.4.1 Experimental design

The experimental design in this study was carried out using Design-Expert version 10.0. The program was used to generate the design matrix based on four process parameters (monomer, comonomer, and ICA pressures, and the polymerization temperature). About 28 experimental runs were generated with a Box-Behnken design (BBD) to evaluate the effects of the selected parameters ethylene pressure (7 – 9 bar), 1-butene pressure (0 – 2 bar), isopentane pressure (0 – 2 bar) and temperature (70 - 90 $^{o}$C) on the output (activity or MFI).

The following equation was used to determine the number of experimental runs ($n$) necessary for the Box-Behnken experimental design:

$$n = 2k^2 - 2k + n_c \quad (1)$$

where $n_c$ is the number of central points and $k$ is the number of components [33].

Table 1. BBD matrix of input factors and polymerization experimental values

| | Input variables | | | | Responses | |
|---|---|---|---|---|---|---|
| Run | PC2 (bar) | P1C4 (bar) | PiC5 (bar) | Temp ($^{o}$C) | MFI (g/10 min) | Activity (kg PE/g cat.h) |
| 1 | 8 | 0 | 1 | 70 | 1.2 | 1.6 |
| 2 | 8 | 0 | 1 | 90 | 3.2 | 1.2 |
| 3 | 8 | 1 | 1 | 80 | 3.6 | 4.2 |
| 4 | 7 | 1 | 1 | 90 | 13.6 | 1.1 |
| 5 | 8 | 1 | 1 | 80 | 3.9 | 4.3 |
| 6 | 7 | 1 | 1 | 70 | 4.4 | 2.5 |
| 7 | 9 | 1 | 1 | 90 | 7.2 | 2.9 |
| 8 | 8 | 1 | 1 | 80 | 3.8 | 4.4 |
| 9 | 8 | 1 | 0 | 90 | 9.5 | 2.5 |
| 10 | 8 | 1 | 2 | 70 | 2.4 | 4.1 |

| | | | | | | |
|---|---|---|---|---|---|---|
| 11 | 8 | 1 | 0 | 70 | 3.9 | 3.4 |
| 12 | 8 | 0 | 0 | 80 | 2.4 | 1.3 |
| 13 | 8 | 2 | 2 | 80 | 6.1 | 6.8 |
| 14 | 7 | 2 | 1 | 80 | 11.1 | 3.4 |
| 15 | 7 | 1 | 0 | 80 | 8.1 | 2.4 |
| 16 | 9 | 0 | 1 | 80 | 1.3 | 1.5 |
| 17 | 7 | 0 | 1 | 80 | 1.4 | 2.5 |
| 18 | 7 | 1 | 2 | 80 | 3.5 | 3.6 |
| 19 | 8 | 0 | 2 | 80 | 0.9 | 2.2 |
| 20 | 8 | 1 | 1 | 80 | 3.7 | 4.1 |
| 21 | 8 | 2 | 1 | 90 | 12.2 | 4.7 |
| 22 | 9 | 1 | 0 | 80 | 2.2 | 3.9 |
| 23 | 9 | 1 | 2 | 80 | 1.9 | 2.1 |
| 24 | 8 | 1 | 2 | 90 | 4.2 | 3.4 |
| 25 | 8 | 2 | 0 | 80 | 11 | 4.8 |
| 26 | 9 | 2 | 1 | 80 | 3.9 | 6.3 |
| 27 | 8 | 2 | 1 | 70 | 7.9 | 5.4 |
| 28 | 9 | 1 | 1 | 70 | 3.1 | 3.4 |

P— pressure, C2—ethylene, 1-C4—1-butene, iC5—iso-pentane, Temp—temperature,

### 2.4.2 ELM-based predictive modeling

The development of the ELM model in this present study was based on one single hidden layer as previously reported [28; 34]. Data scaling is important in machine learning as it improves the accuracy of the predictions. For this reason, the input and output data were scaled (rendered dimensionless) over the range 0 to +1. Furthermore, scaling the data inhibits the network from reaching its local optimum. A straightforward normalization procedure was used in this study to normalize the experimental input and output data [35].

$$N_P = \frac{(P - P_{min})}{(P_{max} - P_{min})} \qquad 2$$

where $P_{min}$ is the input/output parameter's lower bound before normalisation, $P_{max}$ is the input/output parameter's upper limit before normalisation, and $N_P$ is the normalised parameter. The data were also denormalized after the training phase.

For the development of an ELM model, the number of neurons in the hidden layer is crucial because too many or too few neurons can cause overfitting or underfitting of the data, which could prevent the network from successfully recognizing signals and identifying relationships between patterns in the data set. The neurons in the hidden layer were tuned using heuristic

analysis to obtain the best predicted results and the most efficient ELM model. The total number of neurons selected for optimization ranged from 2 to 20. Two subsets of the experimental data (training and testing) were randomly selected for ELM modeling. To train the ELM, a random selection of 70% of the data was used; a second random selection of 30% of the data was used to test the ELM after it had been trained using the weighted parameters obtained during the training phase. Table 2 displays the parameters used to develop the ELM model. MATLAB R2018a was used to develop the ELM model.

A Moore-Penrose generalized inverse was used to calculate output weights. For generalized SLFNs, the output function of the ELM is described as [35; 36]:

$$F_t(y) = \sum_{i=1}^{t} \varphi_i Q(c_i, d_i, y), \qquad c_i \in R^s, \quad d_i \in R^s \tag{3}$$

where the hidden notes learning parameters are $c_i$ and $d_i$. The output node and *i*th hidden note are linked by weight $\varphi_i$. The output value of the ith hidden note for the input $y$ is provided by $Q(c_i, d_i, y)$ which is expressed as

$$Q(c_i, d_i, y) = q\left(\sum_{j=1}^{s} c_{ij} y_j + d_i\right), \quad d_i \in R^s \tag{4}$$

where $i$ is the hidden node with input to $j$ and $c_{ij} = [c_{i1}, c_{i2} \ldots, c_{is}]^T$ is the weight vector connecting the input layer. The *i*th hidden node's bias is expressed as $d_i$ and $y = [y_1, y_2, \ldots, y_s]^T$ is the vector $c_i$'s inner product in $R^s$.

It is possible to find $Q(c_i, d_i, y)$ for the radial basis function (RBF) hidden node with the activation function $q(y)$: $R \to R$ (for instance, Gaussian) given in Eq. (5) by applying Eq. (4) [36]

$$Q(c_i, d_i, y) = q\left(d_i \sqrt{\sum_{j=1}^{s} (y_j - c_{ij})^2}\right)^T, \quad d_i \in R^+ \tag{5}$$

$R^+$ represents the set of all positive real numbers, while $c_i$ and $d_i$ stand in for the node's center and impact factor, respectively. The RBF network is a specific instance of SLFN that includes RBF nodes in its hidden layer. When $S$ number of samples are trained, the ELM's hidden layer output matrix $M$ is presented as :

$$M\begin{bmatrix} m(y_1) \\ \vdots \\ m(y_S) \end{bmatrix} = \begin{bmatrix} Q(c_1, d_1, y_1) & \ldots & Q(c_t, d_t, y_1) \\ \vdots & \vdots & \vdots \\ Q(c_1, d_1, y_N) & \ldots & Q(c_t, d_t, y_N) \end{bmatrix}_{S \times t} \quad 6$$

the target training data matrix ($G$) is given as

$$G = \begin{bmatrix} g_1 \\ \vdots \\ g_S \end{bmatrix}^T \quad 7$$

also the matrix of the output weight is given as

$$\varphi = \begin{bmatrix} \varphi_1 \\ \vdots \\ \varphi_S \end{bmatrix}^T \quad 8$$

Using the Moore-Penrose inversing solution, Eq. (8) can be employed to compute the output given as

$$G = M\varphi \quad 9$$

Table 2. Modeling parameters for ELM and ANFIS

| Model | Property | Value/Comment |
|---|---|---|
| ELM | Minimised error function | MSE |
| | Learning | Supervised |
| | Number of training iterations | 100 |
| | Number of best iterations | 70 |
| | Transfer function | Radia basis (radbas) |
| | Number of tested neurons | 2-20 |
| | Input/output | $4^p/2^q$ |
| | Output weight estimation method | Moore-Penrose generalized inverse |
| ANFIS | Fuzzy type | Sugeno |
| | Input/output | $4^p/1^q$ |
| | Output | 1 |
| | Membership grade shape | Generalized bell-shaped membership function |
| | Input/ouput membership number | 3 |

| | |
|---|---|
| Nodes number | 193 |
| And method | Product |
| Or method | Probabilistic |
| Optimization type | Hybrid |
| Aggregation | Sum |
| Number of rules | 81 |
| Linear/nonlinear parameters | 81/36 |

[p] Ethylene pressure, 1-butene pressure, isopentane pressure and temperature; [q]MFI or activity

**2.4.3 ANFIS-based predictive modeling**.

Using the four input variables, the ANFIS model was implemented using the multiple-input-single-output (MISO) fuzzy model to predict the activity and MFI. The ANFIS model's output was predicted using hybrid learning methods that integrated a defuzzifier algorithm. For each input variable, three generalized bell-shaped membership functions (*gbellmf*) of first order Sugeno fuzzy logic were used. Five layers including normalization, defuzzification, fuzzification, product, as well as the overall summation, were used to build the ANFIS framework [37]. By assuming two input variables with fuzzy inference systems ($r$ and $s$) and an output ($o$), rule 1 and rule 2 can be used to define the Takagi-Sugeno IF-THEN rules with regard to the input variables [37]. For rules 1 and 2, the following expression is provided:

Rule 1: IF $r$ is $R_1$ and $s$ is $S_1$;

THEN $o_1 = a_1 r + b_1 s + c_1$

Rule 2: IF $r$ is $R_2$ and $s$ is $R_2$;

THEN $o_2 = a_2 r + b_2 s + c_2$

If the system outputs are $o_1$, $o_2$ and the fuzzy sets are $R_1$, $R_2$, $S_1$ and $S_2$. The FIS's controllable variables are $a_1$, $a_2$, $b_1$, $b_2$, $c_1$, $c_2$.

(i) First layer

Three input parameters are used by the adaptive nodes in this layer. The next function defines every node $m$.

$$\vartheta_m^1 = \gamma_{R_m}(r) \tag{10}$$

where $\vartheta_m^1$ (symbolizing MF) is the fuzzy set and *r* is the input parameter to node *m*. When the given input n fulfills A, the membership class An is what it suggests. $R_m$ is the membership class that results when the given input *m* satisfies *R*.

The definition of *gbellmf* is as follows:

$$\gamma_{R_m}(r) = \frac{1}{1 + \left|\frac{r - c_m}{a_m}\right|^{2b_m}} \tag{11}$$

where *gbellmf* premise parameters are $a_p$, $b_p$, $c_p$. The width of the curve is modified by *a* and *b* (both must ≥ 0), and *c* is the curve's midpoint. The values of the MFs range from 0 to 1.

(ii) Second layer

There are non-adaptive nodes in this region. In order to scrutinize all the weight ($\sigma$), the incoming signals are processed in this layer. Each output node illustrates the weight's firing power.

$$\vartheta_m^2 = \sigma_m = \gamma_{R_m}(r)_m . \gamma_{S_m}(r), \qquad m = 1,2 \tag{12}$$

(iii) Third layer

This layer computes each level activation rule, and each node executes the necessary fuzzy rules. By dividing each rule's firing power by the total number of rules, this layer is evaluated. The node of this layer is not adaptable.

$$\vartheta_m^3 = \bar{\sigma}_m = \frac{\sigma_m}{\sigma_1 + \sigma_2}, \qquad m = 1,2 \tag{13}$$

(iv) Fourth layer

This layer computes the membership function's output using defuzzification. The nodes of this layer are flexible.

$$\vartheta_m^4 = \bar{\sigma}_m(r_m a + s_m b + c_m), \qquad m = 1,2 \tag{14}$$

where the subsequent parameter set is $[a_m, b_m, c_m]$.

(v) Fifth layer

This contains the sum of each node's defuzzification layer outputs. The output is represented by a single node, which means that the layer is not adaptable.

$$\vartheta_m^5 = \sum_m \bar{\sigma}_m . Q_m \ = \frac{\sum_m \sigma_m . Q_m}{\sum_m \sigma_m}, \qquad m = 1,2 \tag{15}$$

$$Q_m = (r_m a + s_m b + c_m)$$

where $\bar{\sigma}_m . Q_m$ stands for the defuzzification layer's output at node $m$. The ANFIS parameters used in this investigation are listed in Table 2. There are four inputs and two outputs (MFI or activity) in the ANFIS generic block diagram as shown in Figure 1 which also has the tuned FIS's structure (rules). The fuzzy logic toolbox was utilized to model the ANFIS in MATLAB 2018a. The parameters utilized to create the ANFIS model are summarized in Table 2.

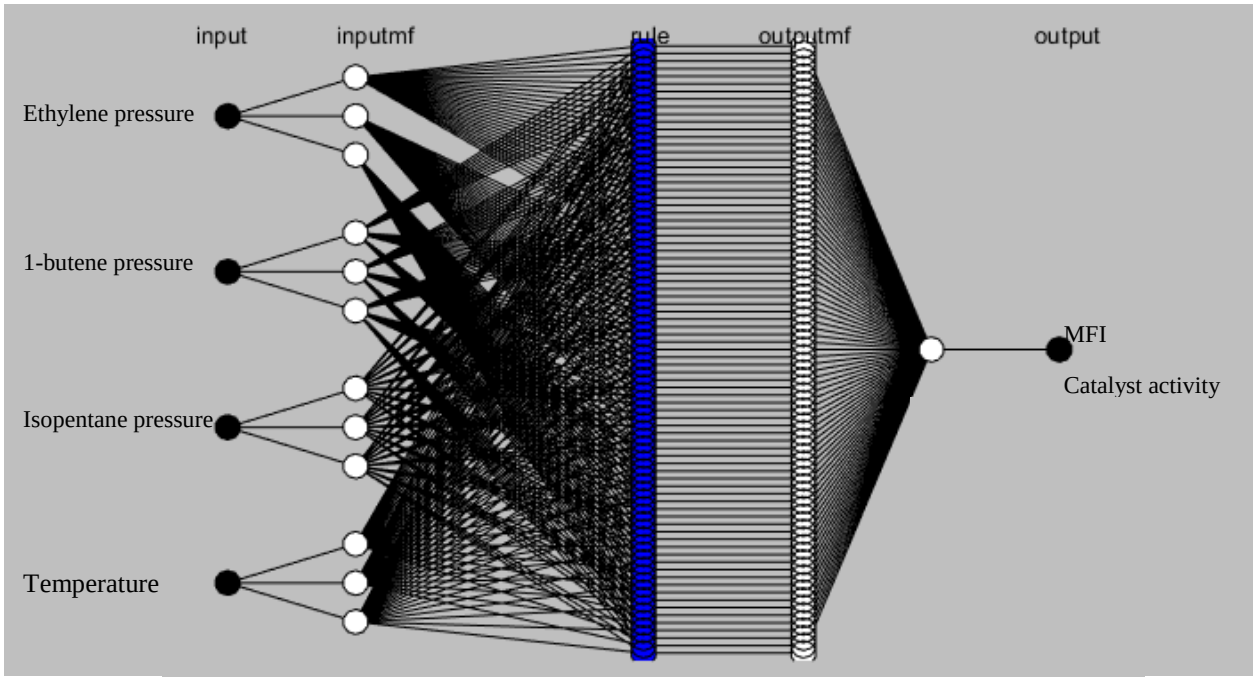


FIGURE 1. ANFIS model structure

### 2.4.4 Input factor sensitivity analysis

Sensitivity analysis shows which inputs or parameters have a significant effect that will determine output variability and hence determines which parameters are strongly correlated with the output. In this work, for the ELM model, the level of significance of the input

variables for the polymerization activity and MFI, which is based on the distribution of weights, was determined using Eq. (16), which was developed by Garson [38]: The estimated weights were used to determine the input variables relative importance.

$$Z_j = \frac{\sum_{\alpha=1}^{\alpha=s_h}\left(\left(\frac{|\Upsilon_{j\alpha}^{ih}|}{\sum_{\beta=1}^{s_i}|\Upsilon_{\beta\alpha}^{ih}|}\right)\times|\Upsilon_{\alpha\tau}^{ho}|\right)}{\sum_{\beta=1}^{\beta=s_i}\left\{\sum_{\alpha=1}^{\alpha=s_h}\left(\frac{|\Upsilon_{\beta\alpha}^{ih}|}{\sum_{\beta=1}^{s_i}|\Upsilon_{\beta\alpha}^{ih}|}\right)\times|\Upsilon_{\alpha\tau}^{ho}|\right\}} \quad (16)$$

where $s_i$ and $s_h$ represent, respectively, the input-hidden neurons. The input, hidden, and output layers are denoted by the superscripts *i*, *h*, and *o*, respectively, while the input, hidden, and output neurons are denoted by the subscripts $\beta$, $\alpha$, and $\tau$. $Z_j$ is the influence of the *j*th input parameter's relative importance on the output. $\Upsilon$ is the weight of the connection.

The highest value of one input variable was determined while maintaining the nominal values (most represented) of the other input variables constant for the sensitivity analysis of the ANFIS model [39; 40]. This ensures an accurate assessment of how input factors impact the outputs (activity or MFI). Table 3 displays the inputs used to build the ANFIS model sensitivity analysis.

Table 3. Sensitivity analysis parameter for the ANFIS model

| Variable | Unit | Nominal | Minimum | Maximum |
|---|---|---|---|---|
| PC2 | bar | 8 | 7 | 9 |
| P1-C4 | bar | 1 | 0 | 2 |
| PiC5 | bar | 1 | 0 | 2 |
| Temperature | $^{o}$C | 80 | 70 | 90 |

### 2.4.5 Performance evaluation of ELM and ANFIS

To assess the performance of the two developed ELM and ANFIS models, statistical analysis was performed. Table 4 displays these statistics, which were determined using Eqs. (17) - (22).

Table 4. Statistics-based metrics for model evaluation.

| S/N | Name | Equations | Number |
|---|---|---|---|
| 1 | Coefficient of correlation | $R = \sqrt{1 - \frac{\sum_{j=1}^{h}(Y^p - Y^e)^2}{\sum_{j=1}^{h}(Y^p - Y_m^e)^2}}$ | 17 |
| 2 | Coefficient of determination | $R^2 = 1 - \frac{\sum_{j=1}^{h}(Y^p - Y^e)^2}{\sum_{j=1}^{h}(Y^p - Y_m^e)^2}$ | 18 |
| 3 | Mean square error | $MSE = \frac{1}{h}\sum_{j=1}^{h}(Y^p - Y^e)^2$ | 19 |
| 5 | Root mean square error | $RMSE = \sqrt{\frac{1}{h}\sum_{j=1}^{h}(Y^p - Y^e)^2}$ | 20 |
| 4 | Mean absolute error | $MAE = \frac{1}{h}\left\|\sum_{j=1}^{h}(Y^p - Y^e)\right\|$ | 21 |
| 5 | Marquart's percentage standard deviation | $MPSD = \frac{100}{h}\left(\sum_{j=1}^{h}\frac{\|(Y^e - Y^p)\|}{Y^e}\right)$ | 22 |

where $Y^e$ is the measured value of output (activity or MFI), $Y^p$ is the predicted value by ELM and ANFIS models, $Y_m^e$ is the average value of $Y^e$, $h$ is the experimental number of points.

## 3.0 RESULTS AND DISCUSSION

### 3.1 Multivariate model analysis with ELM

The complete training of the ELM model in this work was accomplished by choosing the ideal number of neurons, training, and testing the model. Radial basis transfer function (*radbas*) was used to obtain a reliable prediction of the ELM model. Additionally, based on

low MSE and high *R* values for the training and testing, and all datasets, the ideal number of neurons was attained. For both the MFI and the activity, the lowest MSE and highest *R* values for testing, training, and the entire dataset were found in neuron number 12 as illustrated in Figure 2. The scatter graphs in Figure 3 show how the experimental data and predictions from the training, testing, and whole datasets of the ELM relate. The experimental and prognosticated values demonstrate a high correlation, as indicated by the *R* value for the developed ELM model for predicting the activity and the MFI.

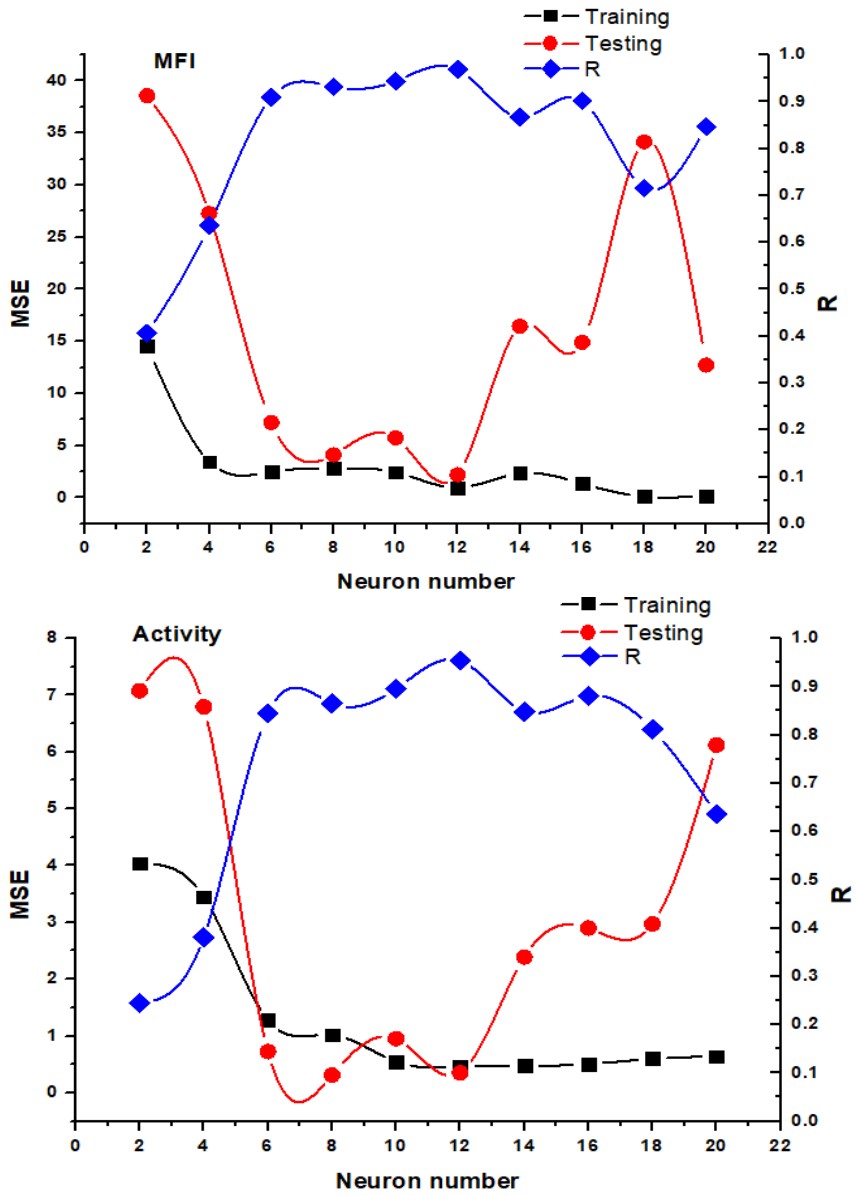


FIGURE 2. The optimal number of hidden neurons for all of the responses investigated.

**MFI**

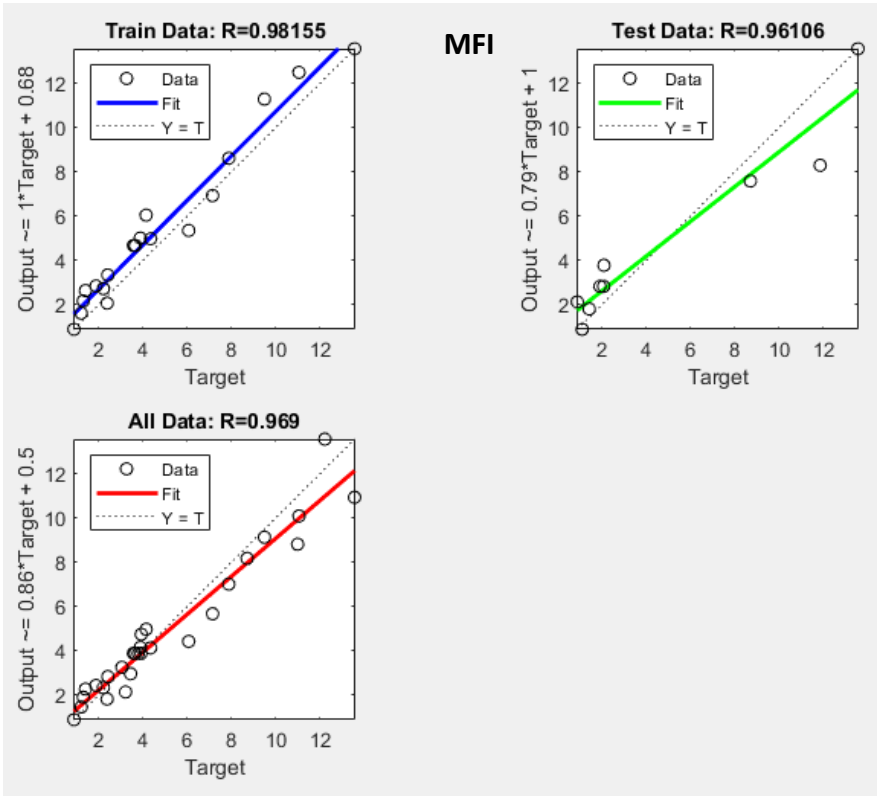


**Activity**

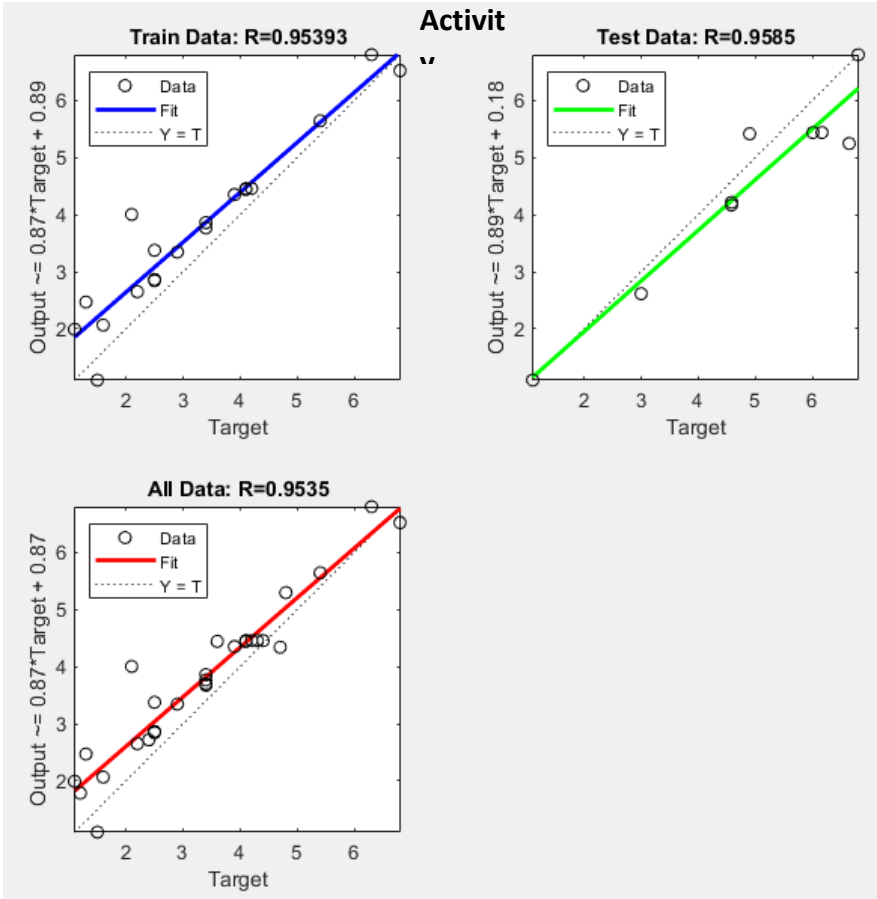

FIGURE 3. Correlation graphs comparing predicted versus measured values.

### 3.2 Multivariate model analysis with ANFIS

The neuro-fuzzy method for the input-output data-based estimation was trained using the BBD data presented in Table 1. To identify the Sugeno type FIS parameters, a hybrid technique that incorporates the least squares approach was used. For each input in this investigation, there were three membership functions. The output component of each rule uses a linear defuzzifier method, and the membership grades used were *gbellmf*. With no error tolerance, a total of 20 epoch iterations were used to train the experimental data for both the activity and MFI. For both outputs (MFI and activity), 81 fuzzy rules, 36 nonlinear parameters, and 193 nodes were utilized. The computed RMSE for the whole dataset was 0.0492 and 0.0423 for the MFI and activity, respectively. The estimated RMSE for activity at the training (0.03536), checking (0.2646), and testing (0.3651) stages as well as the estimated RMSE for MFI during the training (0.0461), checking (0.1699) and testing (0.2887) stages illustrates how reliable the developed ANFIS model is. Figures 4 and 5 support this conclusion. This makes it clear that the developed ANFIS model was able to provide a sufficient prediction of the activity and MFI. The rule viewer for both outputs is shown in Figure 6 and displays the input values and the corresponding computed output. The rule viewer also depicts the trained FIS rules as well as the membership function curves.

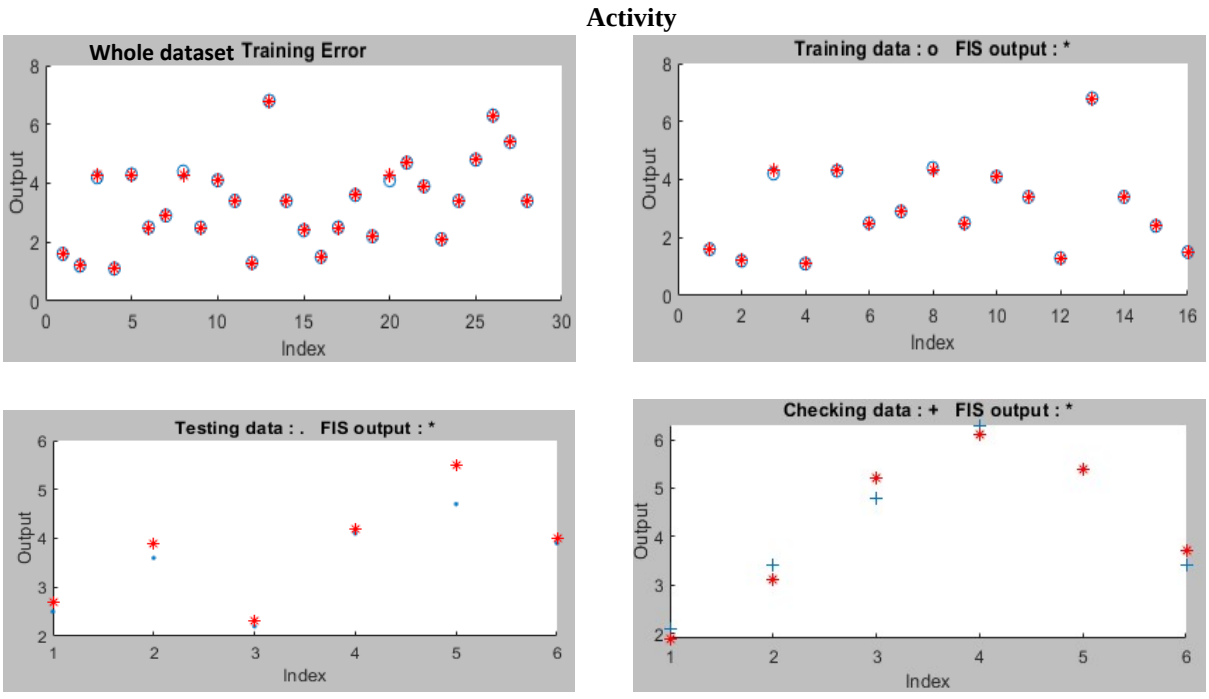

FIGURE 4. Run numbers versus experimental and predicted values for the activity ANFIS model.

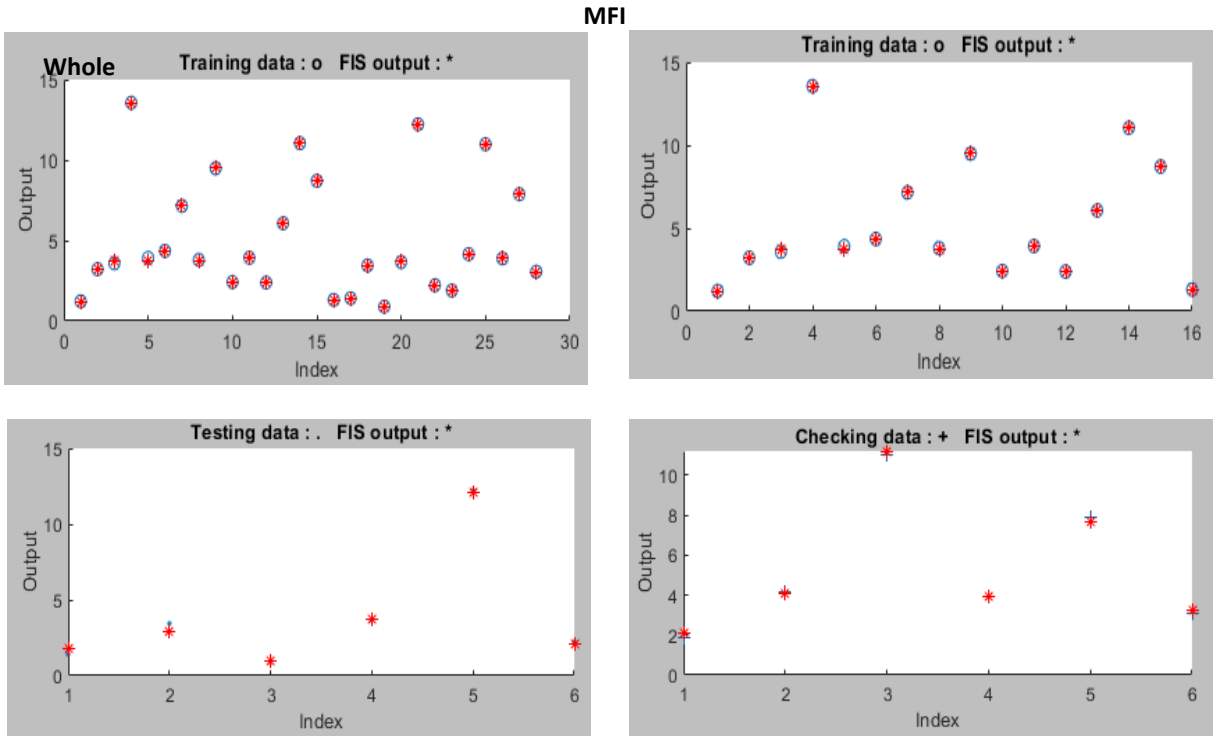


FIGURE 5. Run numbers versus experimental and predicted values for the activity ANFIS model.

### 3.3 Input factors synergistic impact on the MFI

The developed ANFIS models was used to obtain the three-dimensional (3D) surface plots owing to its readily available 3D surface plots toolkit to study the synergistic impact of the various input variables on the corresponding outputs.

It can be seen from the response surface plots of the MFI shown in Figure 7 that as expected, each of the input variables appears to play a significant role in determining the value of the MFI, with the 1-C4 pressure having the largest effect over the studied range and the iC5 pressure having the smallest. The shapes of the surfaces in the Figure 7 show this clearly. These observations have simple logical justifications. The MFI (i.e., a drop in the viscosity average molecular weight) increases with increasing 1-C4 pressure and temperature, as one would anticipate with a Ziegler-Natta catalyst. As greater ethylene concentrations often result in higher molecular weights with Ziegler-Natta catalysts, increasing the C2 pressure causes a

fall in the MFI. Since higher ICA pressures result in more C2 solubility (and diffusivity) in the amorphous phase of the polymer covering the active sites (with respect to comonomer), decreasing iC5 also results in a larger molecular weight [7].

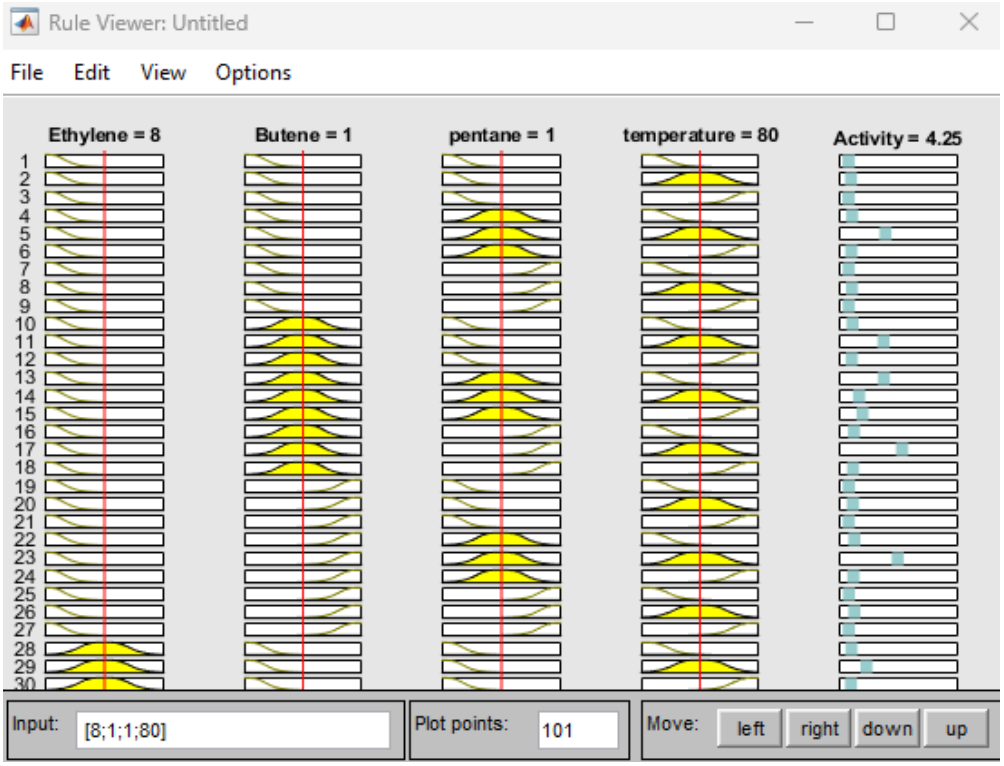


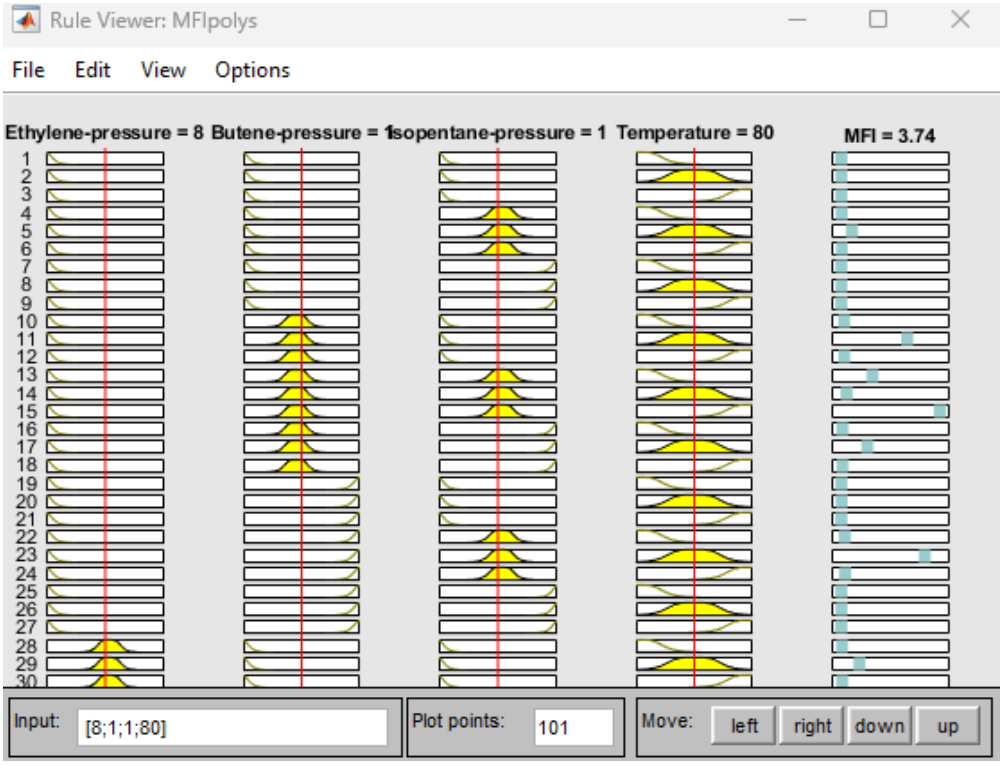

FIGURE 6. Rule view of the developed ANFIS model's input parameters and output (MFI and activity).

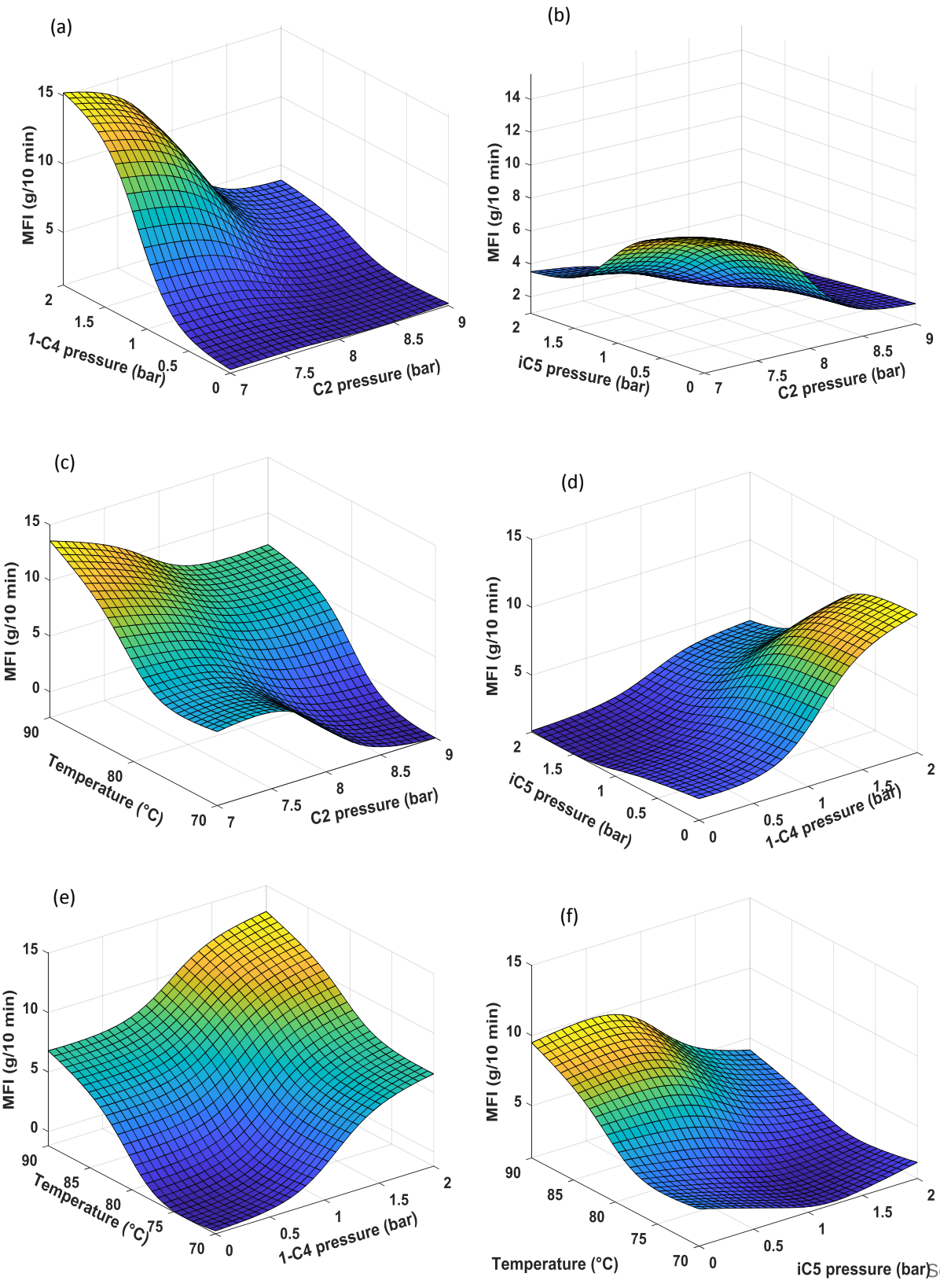

FIGURE 7. Three-dimensional surface plots of MFI as function of (a) C2 and 1-C4 (b) C2 and iC5 (c) C2 and temperature (d) iC5 and 1-C4 (e) 1-C4 and temperature (f) iC5 and temperature

### 3.4 Input factors synergistic impact on the activity.

The interactive effect of the studied input variables on the activity is also illustrated in Figure 8. There is a surge in the activity when iC5 is present in the presence of ethylene. This is because the amorphous phase of the polymer encasing the active sites exhibits greater C2 solubility (and diffusivity) at higher iC5 pressures. The synergistic interaction between C2 and 1-C4 is what should be expected as an increase in the comonomer content triggers the catalyst activity due to the comonomer effect. The other interactive effect as seen from the 3D surface plots shows that strong interaction exists between these variables on the activity.

The 3D surface plots also demonstrate that the presence of at least one alkane is not innocuous. This has been demonstrated by earlier reports from our group, but it is also clear that isopentane interacts with the other process parameters in a significant way, having an impact on both the catalyst activity and the MFI of the resulting polymer. As a result, studying the impact of the choice of induced condensing agents in gas phase polymerization is not simple, and we cannot overlook these chemically inert materials while developing process models.

The goal of the current research is not to provide an exhaustive explanation for these complex interactions, but rather to demonstrate the value of ANFIS and ELM as statistical tools in the field of polyolefin reaction engineering.

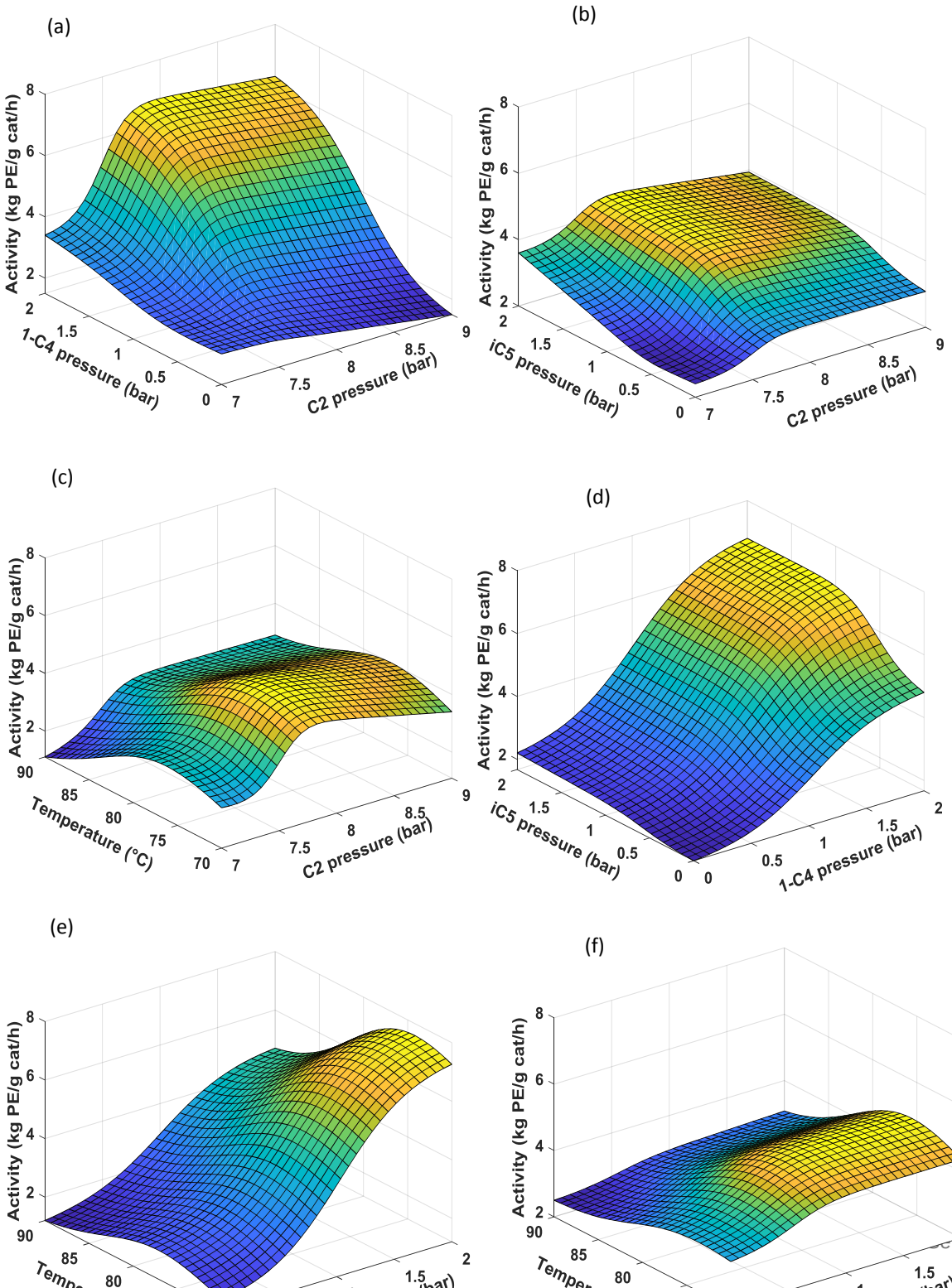

FIGURE 8. Three-dimensional surface plots of activity as a function of (a) C2 and 1-C4 (b) C2 and iC5 (c) C2 and temperature (d) iC5 and 1-C4 (e) 1-C4 and temperature (f) iC5 and temperature

### 3.5 Performance evaluation of the developed models

By employing the overall dataset between the experimental and predicted values from ANFIS and ELM, the models' relative performance for the gas ethylene polymerization process was evaluated using a range of statistics pointers illustrated in Table 4, and the results are displayed in Table 5. Nevertheless, the ANFIS model outperformed the ELM model in terms of $R$ and $R^2$ values. However, it was clear that there was a substantial correlation between the predicted and measured values for both models. The prediction error of a model in relation to the measured value is also assessed by RMSE, MSE, MAE, and MPSD. Comparing the ANFIS model to the ELM model, the ANFIS model showed significantly reduced error levels. The experimental results plotted versus those predicted using the $R^2$ which is shown as Figure S1 of the supporting information lend weight to this finding. The results of the ANFIS model were closer to the trend line than the ELM model's anticipated values. The performance of the developed models might be better understood by plotting the observed and estimated values against the experimental run numbers (Figure 9). Comparing the ANFIS model's predictions to those of the ELM model, the ANFIS model's predictions are noticeably more in line with the experimental data. The superiority of the developed ANFIS model over the developed ELM model in this present work can be attributed to its capacity to combine the ideas of neural networks and fuzzy systems in a single framework.

Table 5. ELM and ANFIS models performance assessment

| | Activity | | MFI | |
|---|---|---|---|---|
| Parameter | ELM | ANFIS | ELM | ANFIS |
| $R$ | 0.9535 | 0.9995 | 0.9690 | 0.9999 |

| | | | | |
|---|---|---|---|---|
| $R^2$ | 0.9092 | 0.9992 | 0.9389 | 0.9998 |
| MSE | 0.3764 | 0.0018 | 0.9081 | 0.0024 |
| RMSE | 0.6135 | 0.0422 | 0.9529 | 0.0493 |
| MAE | 0.4979 | 0.0143 | 0.7106 | 0.0171 |
| MPSD | 46.7912 | 2.2153 | 41.5259 | 2.7471 |

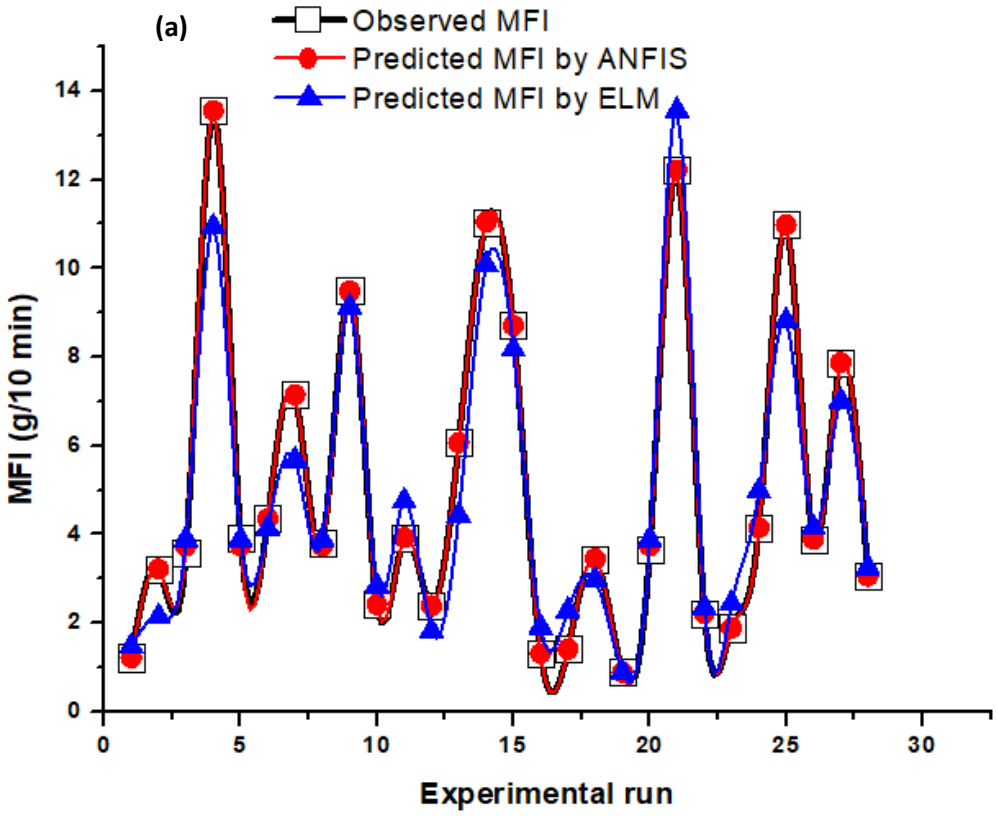


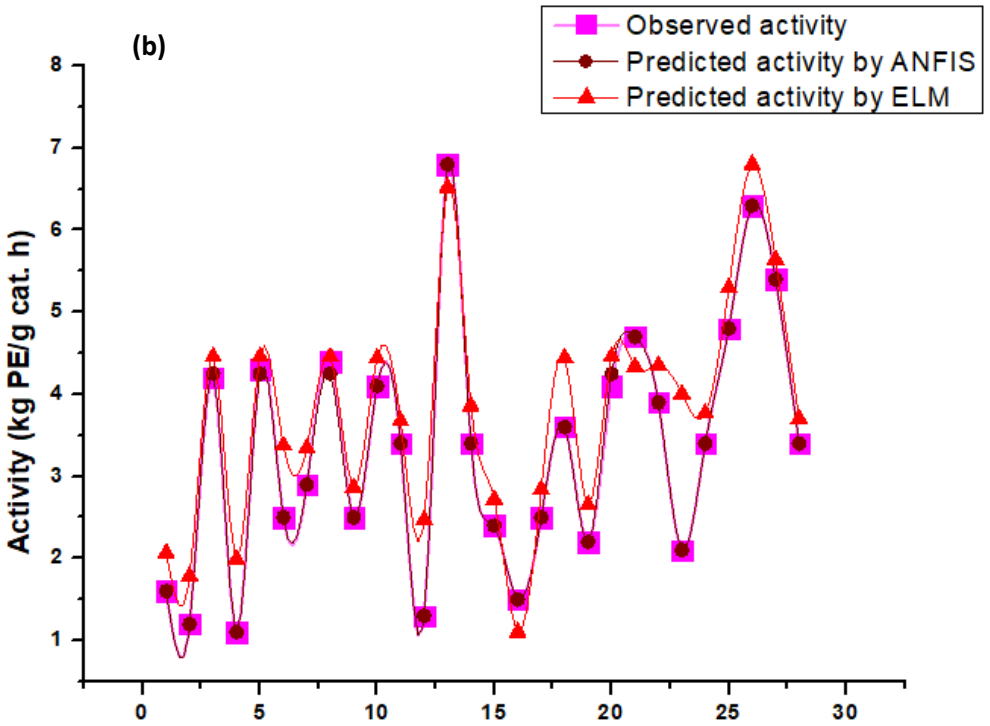

FIGURE 9. Plots comparing experimental runs to predicted and observed values (a) MFI (b) activity

### 3.6 Sensitivity analysis result

Figure 11 shows the outcome of the sensitivity analysis performed on both models, which showed that all operating factors have an impact on MFI and catalyst activity. The figure showed that both models exhibit similar trends in terms of the relative impact of each operating parameter on MFI and catalyst activity despite their different absolute results. The most important operating variable in term of the MFI and the activity is 1-butene pressure, followed by ethylene pressure, then the temperature, and lastly isopentane. Since each operating variable influenced the MFI and catalyst activity yield, it was impossible to discard any of them. The result of the sensitivity analysis has shown that these input parameters are important to produce LLDPE in the range of the condition studied. The addition of isopentane to enhance the heat removal of gas phase polyethylene process cannot be overemphasized.

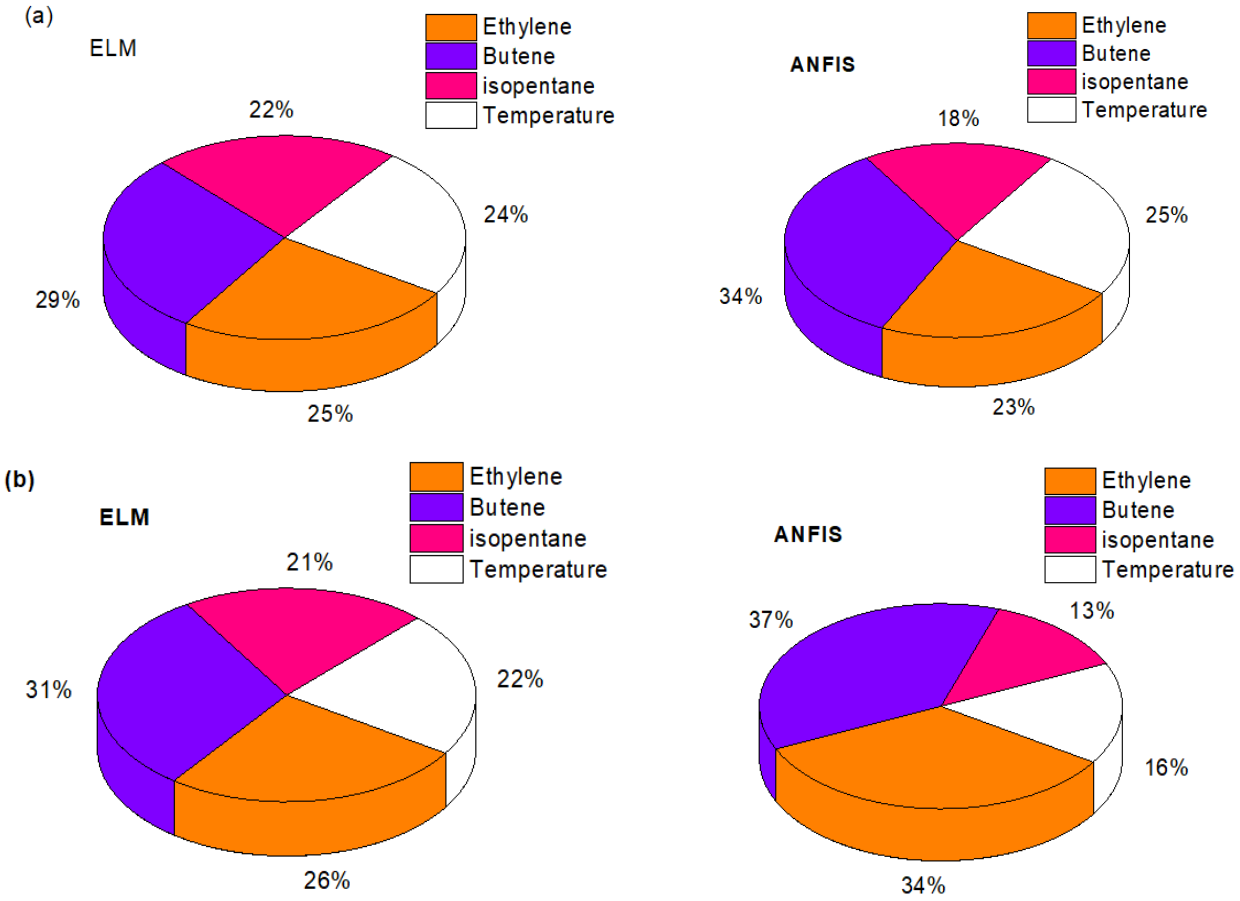

FIGURE 10. Level of influence of process input variables on various output variables (a) MFI (b) activity

## 4 CONCLUSION

This present study investigated the predictive capability of data-driven machine learning tools to wit adaptive neuro-fuzzy inference system (ANFIS) and extreme learning machine (ELM) to predict polymerization kinetics and final polymer properties of gas phase ethylene polymerization using ZN catalyst. The interactive effect of the input factors (ethylene, 1-butene, isopentane pressures, and reaction temperature) on the MFI and catalysts activity was also studied. It was observed that the presence of iC5 as an induced condensing agent has an impact on both outputs. The developed models were statistically adjudged using various statistical indices such as coefficient of correlation ($R^2$) and root mean square error (RMSE). For the MFI, the ANFIS model ($R^2$ = 0.9998, RMSE = 0.0493) performed better than the developed ELM model ($R^2$ = 0.9389, RMSE = 0.9529). In terms of prognosticating the catalyst activity, the ANFIS model ($R^2$ = 0.9992, RMSE = 0.0422) fared better than the ELM model ($R^2$ = 0.9092, RMSE = 0.6135). The ability of the developed ANFIS model to integrate the concepts of neural networks and fuzzy systems into a single framework explains why it outperformed the developed ELM model in this study. Nonetheless, both machine learning tools could predict the MFI and catalyst activity and hence, they are both precise and accurate. In terms of simplicity, the ANFIS model tends to be less complicated to develop in comparison to the ELM model. In addition, the 3D surface plots to study the synergistic impact of the different input factors are easily done with the ANFIS model. All the investigated input factors had a significant impact on the examined responses, according to the developed ANFIS and ELM models sensitivity analysis. None of the variables could have been ignored. The results of the current study show that machine learning technologies may

be effectively used to develop empirical models to predict both the kinetics of polymerization and the properties of the produced polymer.

**Acknowledgment**

NBI thanks the Petroleum Technology Development Fund (PTDF), Nigeria, for their financial support of the doctoral fellowship (Grant Number: 18GFC/PHD/064).

**REFERENCES**

[1] V. Kanellopoulos, C. Kiparissides, *Multimodal Polymers with Supported Catalysts: Design and Production*. **2019**.
[2] https://www.fortunebusinessinsights.com/industry-reports/polyethylene-pe-market-101584 (accessed July 25.
[3] A. Alizadeh, T. F. McKenna, *Macromolecular Reaction Engineering*. **2014**, *8*.
[4] T. F. McKenna, M. A. Bashir, *Multimodal Polymers with Supported Catalysts: Design and Production*. **2019**.
[5] US 4543399. **(1985)**, invs.: J. M. J. Jenkins, R. L.; Jones, T. M.
[6] T. F. McKenna, *Macromolecular Reaction Engineering*. **2019**, *13*.
[7] N. B. Ishola, F. N. Andrade, F. Machado, T. F. McKenna, *Macromolecular Reaction Engineering*. **2020**, *14*.
[8] R. Alves, M. A. Bashir, T. F. McKenna, *Industrial & Engineering Chemistry Research*. **2017**, *56*.
[9] F. N. Andrade, R. Fulchiron, F. Collas, T. F. McKenna, *Macromolecular Chemistry and Physics*. **2019**, *220*.
[10] M. Namkajorn, A. Alizadeh, D. Romano, S. Rastogi, T. F. McKenna, *Macromolecular Chemistry and Physics*. **2016**, *217*.
[11] N. B. Ishola, T. F. McKenna, *Macromolecular Reaction Engineering*. **2022**.
[12] T. F. McKenna, J. B. Soares, *Chemical Engineering Science*. **2001**, *56*.
[13] R. F. Alves, T. F. McKenna, *Chemical Engineering Journal*. **2020**, *383*.
[14] A. Ben Mrad, S. Norsic, N. Sheibat-Othman, T. F. McKenna, *Industrial & Engineering Chemistry Research*. **2021**, *60*.
[15] A. Di Martino, G. Weickert, F. Sidoroff, T. F. McKenna, *Macromolecular Reaction Engineering*. **2007**, *1*.
[16] J. B. Soares, T. F. McKenna, *Polyolefin reaction engineering*, Wiley Online Library, **2012**.
[17] R. G. Brereton, *Chemometrics: data analysis for the laboratory and chemical plant*, John Wiley & Sons, **2003**.
[18] R. H. Myers, D. C. Montgomery, C. M. Anderson-Cook, *Response surface methodology: process and product optimization using designed experiments*, John Wiley & Sons, **2016**.
[19] P. J. DesLauriers, J. S. Fodor, S. Mehdiabadi, V. Hegde, J. B. Soares, *Macromolecular Reaction Engineering*. **2020**, *14*.
[20] P. J. DesLauriers, J. S. Fodor, J. B. Soares, S. Mehdiabadi, *Macromolecular Reaction Engineering*. **2018**, *12*.
[21] C. Georgakis, S.-T. Chin, Z. Wang, P. Hayot, L. Chiang, J. Wassick, I. Castillo, *Industrial & Engineering Chemistry Research*. **2020**, *59*.

[22] H. Nassiri, H. Arabi, S. Hakim, S. Bolandi, *Polymer bulletin*. **2011**, *67*.
[23] N. B. Ishola, T. F. McKenna, *Macromolecular Theory and Simulations*. **2021**, *30*.
[24] T. Charoenpanich, S. Anantawaraskul, J. B. Soares, *Macromolecular Reaction Engineering*. **2016**, *10*.
[25] T. Charoenpanich, S. Anantawaraskul, J. B. Soares, *Macromolecular Theory and Simulations*. **2020**, *29*.
[26] S. Atashrouz, M. Rahmani, Z. Balzadeh, B. Nasernejad, *SN Applied Sciences*. **2020**, *2*.
[27] K. De Smit, T. Wieme, Y. W. Marien, P. H. Van Steenberge, D. R. D'hooge, M. Edeleva, *Reaction Chemistry & Engineering*. **2022**, *7*.
[28] A. S. Silitonga, A. H. Shamsuddin, T. M. I. Mahlia, J. Milano, F. Kusumo, J. Siswantoro, S. Dharma, A. H. Sebayang, H. H. Masjuki, H. C. Ong, *Renewable Energy*. **2020**, *146*.
[29] B. O. Ighose, I. A. Adeleke, M. Damos, H. A. Junaid, K. E. Okpalaeke, E. Betiku, *Energy conversion and Management*. **2017**, *132*.
[30] J. G. Ulloa, *Applied biomedical engineering using artificial intelligence and cognitive models*, Elsevier, **2021**.
[31] A. Yaghoobi, M. Bakhshi-Jooybari, A. Gorji, H. Baseri, *The International Journal of Advanced Manufacturing Technology*. **2016**, *86*.
[32] L. Ezzatzadegan, N. A. Morad, R. Yusof, *Jurnal Teknologi*. **2016**, *78*.
[33] P. Kundu, V. Paul, V. Kumar, I. M. Mishra, *Chemical Engineering Research and Design*. **2015**, *104*.
[34] M. Mujtaba, H. Masjuki, M. Kalam, H. C. Ong, M. Gul, M. Farooq, M. E. M. Soudagar, W. Ahmed, M. Harith, M. Yusoff, *Renewable Energy*. **2020**, *158*.
[35] P. K. Wong, K. I. Wong, C. M. Vong, C. S. Cheung, *Renewable Energy*. **2015**, *74*.
[36] S. Wu, Y. Wang, S. Cheng, *Neurocomputing*. **2013**, *102*.
[37] J.-S. Jang, *IEEE transactions on systems, man, and cybernetics*. **1993**, *23*.
[38] G. D. Garson, *AI expert*. **1991**, *6*.
[39] A. Bassam, O. May Tzuc, M. Escalante Soberanis, L. Ricalde, B. Cruz, *Sustainability*. **2017**, *9*.
[40] N. B. Ishola, A. A. Okeleye, A. S. Osunleke, E. Betiku, *Neural Computing and Applications*. **2019**, *31*.